บทความวิจัย

การปรับเปลี่ยนสมบัติเชิงโครงสร้างและสมบัติเชิงแสงของผลึกนาโนชนิดคอเทอรีอัลลอย $Zn_xHg_{1-x}Se_yS_{1-y}$ ด้วยการคำนวณไทด์บายดิงในระดับอะตอม

วริศรา ทาจิตร์[1] และ วรศักดิ์ สุขบท[1*]
[1]ภาควิชาฟิสิกส์ คณะวิทยาศาสตร์ มหาวิทยาลัยอุบลราชธานี
**Email: w.sukkabot@gmail.com*

รับบทความ: 2 พฤศจิกายน 2564 แก้ไขบทความ: 18 ธันวาคม 2564 ยอมรับตีพิมพ์: 29 มกราคม 2565

บทคัดย่อ

สมบัติทางอิเล็กทรอนิกส์และแสงของผลึกนาโนชนิดคอเทอรีอัลลอย $Zn_xHg_{1-x}Se_yS_{1-y}$ ที่มีพารามิเตอร์ที่สอดคล้องกับการทดลองได้รับการศึกษาด้วยการประมาณค่าผลึกเสมือน (Virtual crystal approximation) ทฤษฎีไทด์บายดิง (Tight-binding theory) และวิธีอันตรกิริยาการกำหนดค่า (Configuration interaction approach) เมื่อค่า x และ y ลดลง ช่องว่างพลังงานลดลง เนื่องจากช่องว่างพลังงานของ HgS ที่มีค่าน้อยมีอิทธิพลเพิ่มขึ้นในผลึกนาโนชนิดคอเทอรีอัลลอย $Zn_xHg_{1-x}Se_yS_{1-y}$ เมื่อเปรียบเทียบผลการคำนวณและผลการทดลองของช่องว่างพลังงาน พบว่า มีความสอดคล้องกัน ประสิทธิภาพทางแสงเพิ่มขึ้นเมื่อค่า x และ y ลดลง และเส้นผ่าศูนย์กลางของผลึกนาโนเพิ่มขึ้น การแบ่งแยกของเอ็กซิตอนแปรผกผันกับเส้นผ่าศูนย์กลางแต่แปรผันตรงกับปริมาณการเจือเนื่องจากอันตรกิริยาแบบเอ็กเซ็งระหว่างอิเล็กตรอนและโฮล (Electron-hole exchange interaction) เมื่อพิจารณากรณีสัดส่วนโดยโมลของ Hg และ S จำนวนมาก การแยกโครงสร้างที่ดีของเอ็กซิตอนจะลดลง ส่งผลให้เป็นตัวแทนที่ดีในการผลิตสถานะพัวพันทางแสง (Entangled photon pair) การเลื่อนไปของความยาวคลื่นแบบสโตกส์ (Stokes shift) เพิ่มขึ้นในกรณีสัดส่วนโดยโมลของ Hg และ S จำนวนมาก ซึ่งสามารถนำไปประดิษฐ์อุปกรณ์กรองทางแสง งานวิจัยนี้ยืนยันว่า ผลึกนาโนชนิดคอเทอรีอัลลอย $Zn_xHg_{1-x}Se_yS_{1-y}$ เป็นสารที่น่าสนใจในการศึกษาสมบัติพื้นฐานและการประยุกต์ใช้ในเทคโนโลยีทางควอนตัม

คำสำคัญ: ทฤษฎีไทด์บายดิง $Zn_xHg_{1-x}Se_yS_{1-y}$ การแยกโครงสร้างที่ดี ช่องว่างพลังงาน ผลึกนาโน

อ้างอิงบทความนี้
วริศรา ทาจิตร์ และวรศักดิ์ สุขบท. (2565). การปรับเปลี่ยนสมบัติเชิงโครงสร้างและสมบัติเชิงแสงของผลึกนาโนชนิดคอเทอรีอัลลอย $Zn_xHg_{1-x}Se_yS_{1-y}$ ด้วยการคำนวณไทด์บายดิงในระดับอะตอม. **วารสารวิทยาศาสตร์และวิทยาศาสตร์ศึกษา**, 5(1), 72-84. http://doi.org/10.14456/jsse.2022.7

Research Article

Structural and optical manipulation of quaternary-alloyed $Zn_xHg_{1-x}Se_yS_{1-y}$ nanocrystals based on atomistic tight-binding theory

Waritsara Thajitr and Worasak Sukkabot*

Department of Physics, Faculty of Science, Ubon Ratchathani University, Thailand, 34190

**Email: w.sukkabot@gmail.com*

Received <2 November 2021>; Revised <18 December 2021>; Accepted <29 January 2022>

Abstract

The fundamental electronic and optical properties of $Zn_xHg_{1-x}Se_yS_{1-y}$ quaternary-alloyed nanocrystals with structural parameters from experimental results are investigated by a virtual crystal approximation (VCA), an atomistic tight-binding description (TB) and configuration interaction approach (CI). With the reducing x and y contents, the optical band gaps are decreased because of the low HgS band gap promoted in $Zn_xHg_{1-x}Se_yS_{1-y}$ quaternary-alloyed nanocrystals. Numerical and experimental optical band gaps appear to agree quantitatively and qualitatively. The optical efficiency is pronounced with the declining elemental compositions (x and y) and increasing diameters. The splittings of excitons are inversely comparative to the diameters, whereas those are directly relational to the alloy compositions as explained by the results of the exchange interaction between electron and hole. On the Hg- and S-rich side, the exciton fine structure splitting is reduced, thus being a good candidate for efficient generation of entangled photon pair. The stokes shift is enhanced in the Zn- and Se-rich side, introducing the excellent pathway for the optical filters. This work confirms that $Zn_xHg_{1-x}Se_yS_{1-y}$ quaternary-alloyed nanocrystals are very interesting systems, not only for fundamental studies but also for future applications of quantum technology.

Keywords: Tight-binding theory, $Zn_xHg_{1-x}Se_yS_{1-y}$, fine structure splitting, band gap, nanocrystals

Cite this article:

Thajitr, W. and Sukkabot, W. (2022). Structural and optical manipulation of quaternary-alloyed $Zn_xHg_{1-x}Se_yS_{1-y}$ nanocrystals based on atomistic tight-binding theory. **Journal of Science and Science Education**, 5(1), 72-84. http://doi.org/10.14456/jsse.2022.7

1. Introduction

Chemical semiconductor nanocrystals have outstanding optoelectronic properties that have been readily tuned through the manipulation of nanocrystal size, shape and surface passivation. Semiconductor nanocrystals smaller than Bohr exciton radius, termed quantum dots (QDs), display size-dependent absorption and emission. The potential applications of nanocrystals have been established in various ways including the utilization as bioimaging, biosensing, light-emitting diodes, photovoltaic devices, lasers and quantum computing devices. (Qi and Gao, 2008; Smith and Nie, 2009; Zrazhevskiy and Gao, 2009; Klimov, et al., 2000; Sun et al., 2007) On top of size and shape control with corresponding spectral tuning, device applications of nanocrystals require accurate control over the electronic alloy. II-VI ternary-alloyed nanocrystals ($A_xB_{1-x}C$) such as CdSeTe, ZnCdSe ZnCdS and CdSSe have been synthesized with the aim to manipulate the structural and optical properties of semiconductors by means of alloy contents x. To overcome the limitation and extend the sensitivity of the alloy tuning, II-VI quaternary-alloyed nanocrystals ($A_xB_{1-x}C_yD_{1-y}$) with x and y tunable compositions are introduced. Mercury chalcogenide (HgX, X = S, Se, Te) nanocrystals are a rich system for the exploration of electronic alloy. These nanostructures have been utilized to create intra-band photodetectors with narrow spectral response in the mid- infrared region (Deng and Guyot-Sionnest, 2016; Shen, et al., 2017; Shen and Guyot-Sionnest, 2016), thus leading to be the scope of interest. For instance, K. Hara et al. (Hara, et al., 1995) synthesized the epitaxial layers of wide-band-gap $Zn_{1-x}Hg_xSe$ (x=0.0-0.14) grown on GaAs substrates. The visible spectral region from blue to red was controlled by changing Hg contents between 0 and 0.06. Using the molecular beam epitaxy, the synthesis of quaternary $Zn_{1-x}Hg_xS_ySe_{1-y}$ (x= 0-0.03, y = 0-0.4) alloy layers coated on GaAs substrates was reported by K. Hara et al. (Hara, et al., 1996; Hara, et al., 1998) These alloy layers might be utilized for practical blue-green laser applications. The synthesis of CdS, $Zn_yCd_{1-y}S$, and $Hg_yCd_{1-y}S$ nanoparticles with size- and composition-dependent optical features was carried out by Brian A. Korgel (Korgel and Monbouquette, 2000) These nanostructures showed the well-defined optical spectra. The short-range principle of the charge carrier scattering processes on the various lattice defects in the ZnCdTe, ZnHgSe and ZnHgTe solid solutions was informed by Orest P. Malyk (Malyk, 2009). A good agreement between theory and experimental data in the investigated temperature range was presented. Guo-Yu Lan et al. (Lan, et al., 2010) described the synthesis of highly water-soluble $Zn_xHg_{1-x}Se_yS_{1-y}$ nanocrystals in aqueous solution. $Zn_xHg_{1-x}Se_yS_{1-y}$ quantum dots emitted wavelengths ranging from the UV to the near-IR region (405-760 nm). According to the previous literatures, there were widespread experimental studies, whereas there is no theoretical work. Here, $Zn_xHg_{1-x}Se_yS_{1-y}$ quaternary-alloyed nanocrystals are used as the simulation candidates.

The key principle behind this new work is to understand the structural and optical properties of $Zn_xHg_{1-x}Se_yS_{1-y}$ nanocrystals and then provide the detailed information for the potential applications. In addition, we focus my attention on the stokes shift and excitonic fine structure splitting of $Zn_xHg_{1-x}Se_yS_{1-y}$ nanocrystals. According to the previous investigations, there has been neither theoretical nor experimental research studied in this field. Computations of natural properties of innovative nanostructures must offer atomistic accuracy with an available computational complication. In this work a numerical answer to this problem with the essentials of the atomistic modelling is presented. The atomistic tight-binding method with the inclusion of five orbitals sp^3s^* per atom, the first nearest neighbouring interaction and spin-orbit coupling (Vogl, et al., 1983) is used as the numerical model. Under the alloyed concentrations (x and y) in $Zn_xHg_{1-x}Se_yS_{1-y}$ nanocrystals, the revised version of the virtual crystal approximation (VCA) (Garcıa, et al., 2000) in the presence of the empirical bowing parameters is considered. This technique has been used to successfully study the structural and optical properties of alloy nanostructures (Mourad and Czycholl, 2010; Nestoklon, et al., 2016; Boykin, 2009; Boykin, et al., 2007). Here, the numerical results of quaternary-alloyed $Zn_xHg_{1-x}Se_yS_{1-y}$ nanocrystals with the experimentally synthesized compositions (x and y) and diameters are used as a demonstration.

By means of an atomistic tight-binding and configuration interaction technique, the paper provides the investigations on the single particle spectra and excitonic splitting of $Zn_xHg_{1-x}Se_yS_{1-y}$ quaternary-alloyed nanocrystals. The aim is to identify and to analyze size and composition dependence on the electronic structures, optical properties and excitonic splitting in such alloy nanoclusters. The paper is organized as follows. In section 2, the computational methods are described by the step-by-step solution to this problem. In section 3, the computational results for the electronic structures of $Zn_xHg_{1-x}Se_yS_{1-y}$ quaternary-alloyed nanocrystals computed with this model are compared with the experimental values. The tight-binding band gaps are in a qualitative agreement with synthesized data. In the same section, we also show the excitonic splittings of $Zn_xHg_{1-x}Se_yS_{1-y}$ quaternary-alloyed nanocrystals under several structural parameters. These splittings are of fundamental importance for potential applications in optoelectronics and quantum technology. Finally in section 4, we finish with the conclusions.

2. Theory and Methodology

To achieve this objective, atomistic tight-binding method is implemented and utilized. This approach origins from the Slater-Koster scheme (Slater and Koster, 1954). Tight-binding matrix elements are described by several empirical parameters that can fit and provide the good bulk properties for instance effective masses and band gaps in the comparison with density functional theory and experiments. The tight-binding method applied to a nanocluster problem generates a Hamiltonian matrix with dimensions extending to 10^3. Due to the advantage in the nearest-neighbouring approximation, the sparse matrix is obtained. For selected single particle spectra closed to energy band gap, the eigenvalue problem is solved efficiently using PReconditioned Iterative MultiMethod Eigensolver (PRIMME) (Stathopoulos and McCombs, 2010; Wu, et al., 2017). Using the experimental parameters (Lan, et al., 2010), we consider the $Zn_xHg_{1-x}Se_yS_{1-y}$ quaternary-alloyed nanocrystals with zinc-blende structure. For instance, $Zn_{0.98}Hg_{0.02}Se_{0.64}S_{0.36}$, $Zn_{0.96}Hg_{0.04}Se_{0.60}S_{0.40}$, $Zn_{0.90}Hg_{0.10}Se_{0.56}S_{0.44}$ and $Zn_{0.88}Hg_{0.12}Se_{0.44}S_{0.56}$ nanocrystals are used as the computational candidates labelled as Sample 1 - Sample 4, respectively. For the surface passivation, the energy shift is terminated at the surface as described by S. Lee et al. (Lee, et al., 2004) Once the atomic positions are obtained, we utilize them to calculate single particle spectra by the empirical tight-binding model accounting for spin-orbit coupling and nearest-neighbouring interactions. In the next step of calculation, the single particle states relate to the quantities treated as empirical parameters. An atomic orbitals are in the linear combination forming the tight-binding wave functions given by:

$$\Psi = \sum_{\vec{R}a} C_{\vec{R}a}^{\nu} \left| \vec{R}a \right\rangle$$

All atomic positions R are termed by the summation, α is the (spin) orbital index and $C_{\vec{R}a}^{\nu}$ is the eigenfunction in the $\left| \vec{R}a \right\rangle$ basis. Using the language of the second quantization, the tight binding Hamiltonian for a nanocrystal consisting of N atoms is given as:

$$H_{TB} = \sum_{i=1}^{N}\sum_{\alpha=1}^{10} \varepsilon_{i\alpha} c_{i\alpha}^{\dagger} c_{i\alpha} + \sum_{i=1}^{N}\sum_{\alpha=1}^{10}\sum_{\alpha'=1}^{10} \lambda_{i\alpha\alpha'} c_{i\alpha}^{\dagger} c_{i\alpha'} + \sum_{i=1}^{N}\sum_{i'=1}^{N}\sum_{\alpha=1}^{10}\sum_{\alpha'=1}^{10} t_{i\alpha,i'\alpha'} c_{i\alpha}^{\dagger} c_{i'\alpha'}$$

For the demonstration, $c_{i\alpha}^{\dagger}(c_{i\alpha})$ is the creation (annihilation) of electron on (spin) orbital α centered on i^{th} atom. $\varepsilon_{i\alpha}$ and $t_{i\alpha,i'\alpha'}$ are correspondingly onsite (atomic) energies and offsite (hopping) parameters. $\lambda_{i\alpha\alpha'}$ is the spin-orbit effect. In practical calculations, the parameter set ($\varepsilon_{i\alpha}$, $t_{i\alpha,i'\alpha'}$ and $\lambda_{i\alpha\alpha'}$) was taken from Olguin et al. (Olguin, et al., 2001) In the presence of x and y alloy compositions in $Zn_xHg_{1-x}Se_yS_{1-y}$ quaternary-alloyed semiconductor, the virtual crystal approximation (VCA) is used to produce the tight-binding parameters (P) as given by:

$$P_{Zn_xHg_{1-x}Se_yS_{1-y}} = xyP_{ZnSe} + x(1-y)P_{ZnS} + (1-x)yP_{HgSe} + (1-x)(1-y)P_{HgS}$$

In the alloy semiconductors, the band gaps are non-linear dependent on the compositions. Therefore, the empirical bowing parameters are considered by modifying the s orbital one-site terms (Garcıa et al., 2000).

The electronic structures of single particles states are obtained by the tight-binding calculations. Finally, we follow the single-particle calculation with a many-body calculation to obtain the excitonic splitting and in particular excitonic fine structure. The Hamiltonian for the single exciton (electron-hole pair) is equated in second quantization as:

$$\mathbf{H} = \sum_{i} \mathbf{E}_i \mathbf{e}_i^{\dagger} \mathbf{e}_i + \sum_{j} \mathbf{E}_j \mathbf{h}_j^{\dagger} \mathbf{h}_j - \sum_{ijkl} \mathbf{V}_{ijkl}^{eh,coul} \mathbf{h}_i^{\dagger} \mathbf{e}_j^{\dagger} \mathbf{e}_k \mathbf{h}_l + \sum_{ijkl} \mathbf{V}_{ijkl}^{eh,exch} \mathbf{h}_i^{\dagger} \mathbf{e}_j^{\dagger} \mathbf{e}_k \mathbf{h}_l$$

The energies related to electron and hole are described in the first-two terms, respectively. The atomistic coulomb and exchange interaction of electron-hole pair are symbolized in the third and fourth term. The single exciton Hamiltonian is expanded in a basis of electron-hole configurations constructed from several lowest electron and highest hole states. This approach is widely acknowledged as the configuration interaction technique (CI) or the exact diagonalization approach (Korkusinski and Hawrylak, 2013; M. Zielinski, 2013; Reboredo, et al., 2000; De Oliveira, et al., 2012; Sukkabot, 2016; Sukkabot, 2016; Sukkabot 2016).

3. Results and discussions

Now we proceed to analyze and describe the influence of the diameters and alloying contents (x and y) on electronic structures, optical behavior, atomistic electron-hole interactions and excitonic splitting in $Zn_xHg_{1-x}Se_yS_{1-y}$ experimentally synthesized nanocrystals. Two anion atoms (Se with content y and S with content 1-y) and two cation atoms (Zn with concentration x and Hg with concentration 1-x) with the diameters D_C are combined to be the quaternary-alloyed nanocrystals. Using the structural parameters synthesized by Lan et al. (Lan, et al., 2010), $Zn_{0.98}Hg_{0.02}Se_{0.64}S_{0.36}$, $Zn_{0.96}Hg_{0.04}Se_{0.60}S_{0.40}$, $Zn_{0.90}Hg_{0.10}Se_{0.56}S_{0.44}$ and $Zn_{0.88}Hg_{0.12}Se_{0.44}S_{0.56}$ nanocrystals with zinc-blende structure are used as the simulated candidates with Sample 1 - Sample 4, respectively. Table 1 demonstrates the number of atoms in all Samples under different diameters. The number of atoms mainly depends on the sizes of quaternary-alloyed nanocrystals, while there is no alloying effect on the number of atoms. The empirical tight-binding (TB), modified virtual crystal approximation (VCA) and configuration interaction (CI) scheme are utilized as the atomistic modeling. Let us start with the single-particle spectra under various alloying compositions and diameters. For the demonstration, Figure 1 displays the electron and hole energies of $Zn_xHg_{1-x}Se_yS_{1-y}$ quaternary-alloyed nanocrystals as a function of contents (x and y) and diameters. The energies of e_2 states are slightly different with those of e_3 and e_4 states. In addition, e_3 and e_4 states are degenerate. This is due to the fact that these states are mainly from p orbitals. With the decreasing compositions (x and y), the energies of electron states tend to reduce but those of hole states are mostly increased. In term of increasing diameters, the energies of electron levels are decreased, while those of hole levels are enhanced. To provide a very good description of the optoelectronics properties, Figure 2 exemplifies the optical band gaps of $Zn_xHg_{1-x}Se_yS_{1-y}$ quaternary-alloyed nanocrystals under various elemental concentrations (x and y) and diameters. These calculations show that it is probable to modify the band gaps by control of diameters and contents. With the reduction of x and y contents, the optical band gaps tend to decrease. This can be attributed to the low HgS band gap promoted in $Zn_xHg_{1-x}Se_yS_{1-y}$ quaternary-alloyed nanocrystals. In tight-binding model, the band gaps of ZnSe and HgS semiconductor are 2.82 eV and 0.20 eV, respectively. The non-monotonic reduction of the optical band gaps as the decreasing x and y compositions may be arisen from the non-linear tight-binding parameters obtained by the virtual crystal approximation (VCA). The decrease of optical band gaps is displayed with the growing diameters, as can be understood by the quantum confinement. In addition, we compare the band gaps of our calculation results for the 4.00 nm nanocrystals with those obtained experimentally. Numerical and experimental data appear to agree well for $Zn_xHg_{1-x}Se_yS_{1-y}$ quaternary-alloyed nanocrystals. The

inconsistency may be occurred from the size dispersion in the experiment (Lan, et al., 2010). We reveal that a visible spectral region can be achieved in $Zn_xHg_{1-x}Se_yS_{1-y}$ nanocrystals by controlling diameters and alloying concentrations (x and y), which is auspicious for photovoltaics and photosensor applications. Besides, 2D charge densities of ground-state electron and hole in xy plane under different samples and diameters are displayed in Figure 3 and 4, respectively. The charge densities of electron and hole are localized in the center of $Zn_xHg_{1-x}Se_yS_{1-y}$ nanocrystals. The electron and hole charge densities of $Zn_xHg_{1-x}Se_yS_{1-y}$ nanocrystals with diameter of 4.00 nm expansively more spread outward to the surface than those with diameter of 2.00 nm. On the other hand, there is no dependence of elemental contents on the electron and hole charge densities. Therefore, alloy compositions and diameters have been established as the key factors affecting qualitatively the electronic structures of $Zn_xHg_{1-x}Se_yS_{1-y}$ quaternary-alloyed nanocrystals.

Table 1 The number of atoms in each Sample

Sample ($Zn_xHg_{1-x}Se_yS_{1-y}$)	Number of atoms	
	D_c = 2.0 nm	D_c = 4.0 nm
1 ($Zn_{0.98}Hg_{0.02}Se_{0.64}S_{0.36}$)	191	1551
2 ($Zn_{0.96}Hg_{0.04}Se_{0.60}S_{0.40}$)	191	1551
3 ($Zn_{0.90}Hg_{0.10}Se_{0.56}S_{0.44}$)	191	1551
4 ($Zn_{0.88}Hg_{0.12}Se_{0.44}S_{0.56}$)	191	1551

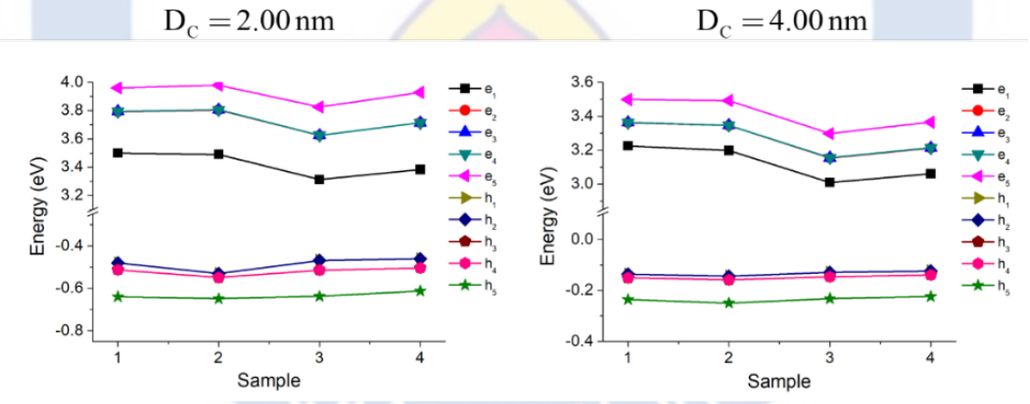

Figure 1 Single-particle spectra of quaternary-alloyed $Zn_xHg_{1-x}Se_yS_{1-y}$ nanocrystals under different samples and diameters.

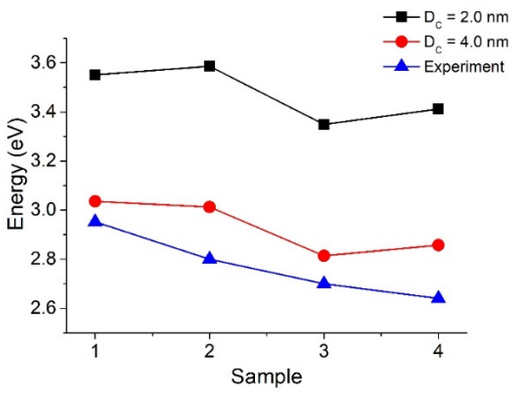

Figure 2 Optical band gaps of quaternary-alloyed $Zn_xHg_{1-x}Se_yS_{1-y}$ nanocrystals under different samples and diameters. The experiment was carried out by Lan et al. (Lan, et al., 2010)

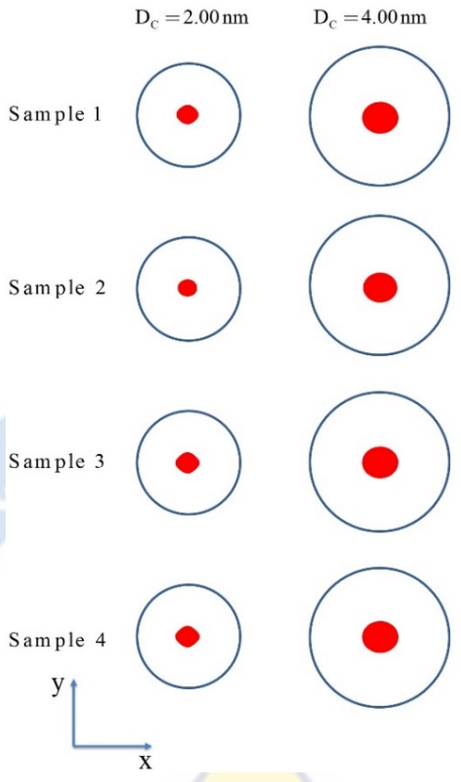

Figure 3 Electron charge densities of quaternary-alloyed $Zn_xHg_{1-x}Se_yS_{1-y}$ nanocrystals under different samples and diameters in xy plane. Circles represent the nanocrystals. The charge density levels are chosen as 0.70 of the maximum probability density.

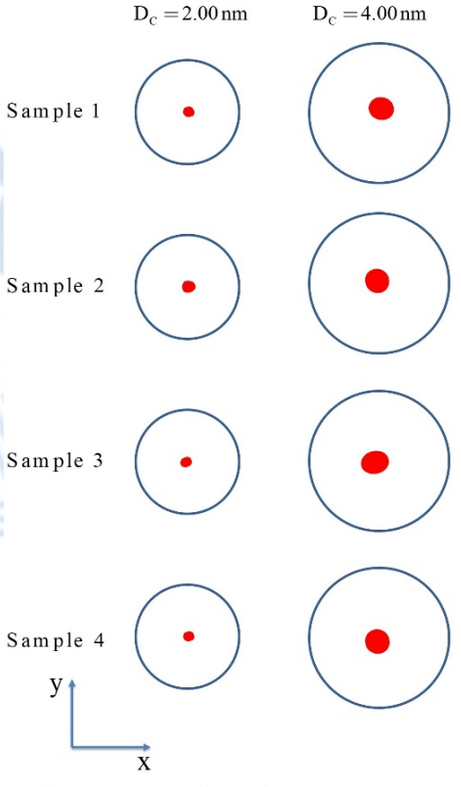

Figure 4 Hole charge densities of quaternary-alloyed $Zn_xHg_{1-x}Se_yS_{1-y}$ nanocrystals under different samples and diameters in xy plane. Circles represent the nanocrystals. The charge density levels are chosen as 0.70 of the maximum probability density.

Likewise, the first electron-hole wave function overlap is performed to detect changes in the excitonic splitting in quaternary-alloyed $Zn_xHg_{1-x}Se_yS_{1-y}$ nanocrystals (Efros, et al., 1996). The overlaps of the ground-state electron-hole wave functions directly depend on the splitting of the excitonic states. The overlaps of the ground-state electron-hole wave functions equate to $\left\langle \Psi^{h=1} \middle| \Psi^{c=1} \right\rangle$ where $\Psi^{c=1}$ and $\Psi^{h=1}$ are the ground electron and hole wave function. Taking the elemental contents (x and y) and diameters into account, the ground electron and hole wave function overlaps are showed in Figure 5. The overlaps of ground electron and hole wave functions are gradually reduced with the decreasing alloy contents (x and y), while those are increased greatly with the decreasing diameters. These behaviours can be clarified by 2D charge densities of ground-state electron and hole in Figure 3 and 4. This tendency will describe the behaviours of the excitonic splitting in the succeeding. The next goal is an attempt to answer the key question related to optical properties in the existence of the alloy contents and sizes. Figure 6 displays the ground-state oscillator strengths of quaternary-alloyed $Zn_xHg_{1-x}Se_yS_{1-y}$ nanocrystals with different compositions (x and y) and diameters. The ground-state oscillator strength is computed via $\frac{2m_0}{\hbar^2}\left|\hat{e}\vec{D}_{eh}\right|^2 \times \left(E_e - E_h\right)$. m_0 is the free-electron mass. E_e and E_h are the ground electron and hole energies, respectively. The vector of the polarization ($\hat{e}$) in the xy plane [110] is used. $\vec{D}_{ij}$ are the dipole moments between ground-state transition. There is a drastic increase in the oscillator strengths with the decreasing elemental compositions (x and y) and increasing diameters. Therefore, the optical effectiveness is promoted in Zn-rich and Se-rich $Zn_xHg_{1-x}Se_yS_{1-y}$ nanocrystals with a large diameter, hence deserving for the optoelectronic devices.

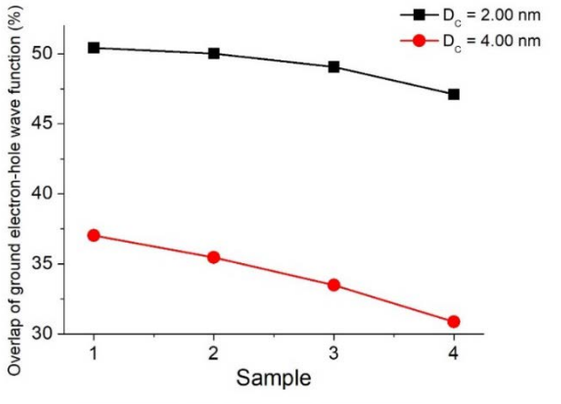

Figure 5 Ground electron-hole wave function overlaps of quaternary-alloyed $Zn_xHg_{1-x}Se_yS_{1-y}$ nanocrystals under different samples and diameters.

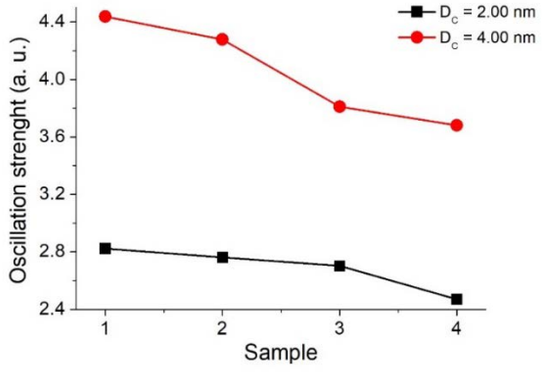

Figure 6 Ground-state oscillation strengths of quaternary-alloyed $Zn_xHg_{1-x}Se_yS_{1-y}$ nanocrystals under different samples and diameters.

It is also enlightening to look at the influence of diameters and compositions (x and y) on the atomistic electron-hole interactions. The description of coulomb and exchange integrals calculated from the tight-binding wave functions is described in more detail in these papers (Sheng, et al., 2005; Schulz, et al., 2006; Zielinski, et al., 2010). The energies of ground-state coulomb and exchange interaction under different diameters and alloy contents (x and y) are schemed in Figure 7 and 8, respectively. With the increasing diameters, the energies of electron-hole coulomb interaction are decreased. This means that the weak confinement of electron-hole pair is realized in the large nanocluster. There is no perturbation of electron-hole coulomb interaction by the alloy contents. To analyze the electron-hole exchange interaction under structural parameters, let us first move back to the intersection of the electron-hole wave function and utilize them to describe this tendency. The exchange interaction between electron-hole pair is decreased with the growing diameters owing to the pattern of the electron-hole wave function overlaps. Additionally, the energies of this interactions are gradually decreased with the reduction of alloy contents because of the configuration of the electron-hole wave function overlaps. The behaviours of the excitonic splitting is explained by the exchange interaction between electron-hole pair subsequently. These computations illuminate that these structural constraints are the key factors to qualitatively analyze the atomistic electron-hole interactions.

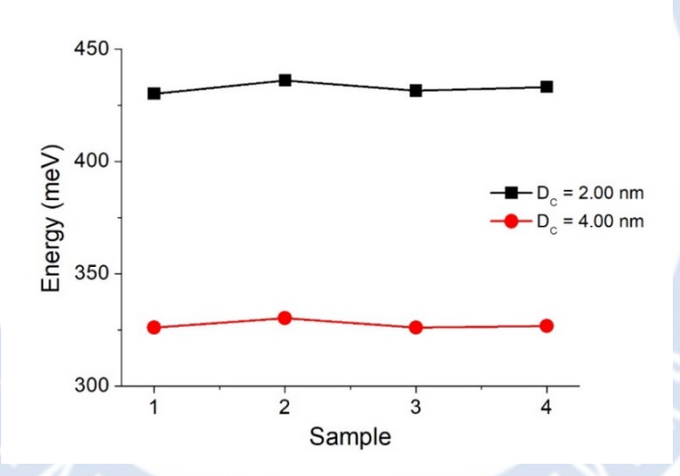

Figure 7 Electron-hole coulomb energies of quaternary-alloyed $Zn_xHg_{1-x}Se_yS_{1-y}$ nanocrystals under different samples and diameters.

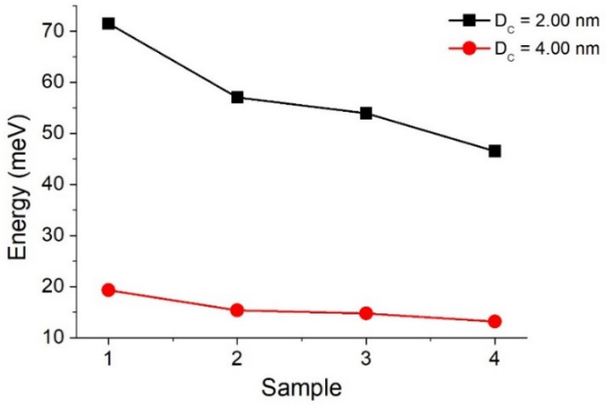

Figure 8 Electron-hole exchange energies of quaternary-alloyed $Zn_xHg_{1-x}Se_yS_{1-y}$ nanocrystals under different samples and diameters.

As mentioned in the introduction, the applications of the quaternary-alloyed $Zn_xHg_{1-x}Se_yS_{1-y}$ nanocrystals are also presented. The polarization-entangled photon pairs were initially proposed by Benson et al. (Benson, et al., 2000) using the biexciton (XX) → exciton (X) → ground state (0) cascade process. In the presence of the anisotropic electron-hole exchange interaction, the splitting of the exciton states (X) is presented. The splitting between the dark and bright excitonic energies, namely stokes shift, is instigated for the optical filters (Butler, 2011). The splitting between these bright excitonic states, called fine structure splitting, terminates the entangled photon generation. These splittings of excitons are directly proportional to the electron-hole exchange interaction. Understanding the physical mechanisms of the bright excitonic splitting is thus indispensable for quantum technology. According to the literature, there has been neither theoretical nor experimental work done in the quaternary-alloyed $Zn_xHg_{1-x}Se_yS_{1-y}$ nanocrystals. Solving by the configuration interaction method (CI), the two-body Hamiltonian is extended in a product of electron-hole configurations from 12 lowest single particle electron and hole levels with spin-up and -down components. The dark-bright (stokes shift) and bright-bright (fine structure splitting) excitonic splitting of $Zn_xHg_{1-x}Se_yS_{1-y}$ nanocrystals are displayed as a function of diameters and alloy content (x and y) in Figure 9 and 10, respectively. The splittings of excitons are inversely relational to the diameters due to the exchange interaction between electron-hole pair. The excitonic splittings are reduced when the alloy contents are decreased, described by the outcomes of the electron-hole exchange interaction. On the Hg- and S-rich side, the reduced fine structure splitting is realized as a key prerequisite for efficient entangled photon pair generation. On contrary, the pronounced stokes shift is presented in the Zn- and Se-rich side, introducing the pathway for the excellent optical filters. Under the optimized structural parameters, vanishing bright exciton fine structure in $Zn_xHg_{1-x}Se_yS_{1-y}$ quaternary-alloyed nanocrystals may have the applications in entangled photon generation, whereas the enlargement of stokes shift may allow for efficient utilization of optical filter.

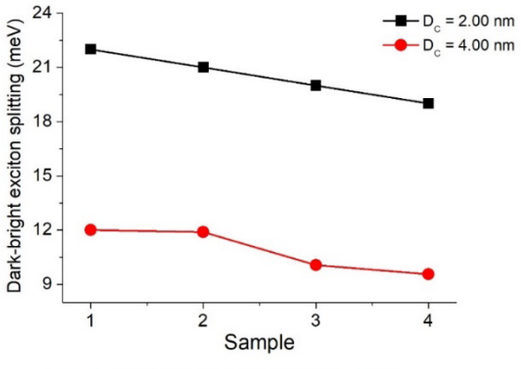

Figure 9 Dark-bright exciton splitting of quaternary-alloyed $Zn_xHg_{1-x}Se_yS_{1-y}$ nanocrystals under different samples and diameters.

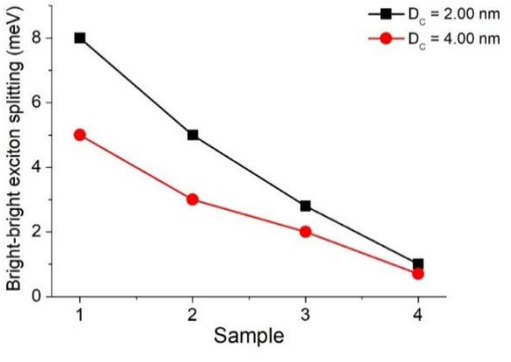

Figure 10 Bright-bright exciton splitting of quaternary-alloyed $Zn_xHg_{1-x}Se_yS_{1-y}$ nanocrystals under different samples and diameters.

4. Conclusion

Inspired by such techniques, the atomistic tight-binding calculations of the electronic structures and optical properties in the quaternary-alloyed $Zn_xHg_{1-x}Se_yS_{1-y}$ nanocrystals with synthesized parameters are demonstrated. These calculations point out that it is in principle possible to tailor the natural properties of these alloy nanocrystals by the control of diameters and elemental compositions. The optical band gaps corresponding to the visible wave lengths are manipulated by changing the diameters and alloy contents (x and y), which is promising for photovoltaics and photosensor implementations. The good consistency of optical band gaps between the atomistic tight-binding approach and experiment is successfully realized. Theoretical modeling underlines that the energies of ground-state electron-hole coulomb and exchange interaction depend on the diameters and elemental compositions. The splittings of excitonic states are inversely proportionate to the diameters, whereas those are directly proportional to the alloy compositions. The excitonic fine structure splitting on the Hg- and S-rich side of $Zn_xHg_{1-x}Se_yS_{1-y}$ nanocrystals is reduced, thus introducing to a good candidate for generation of quantum entanglement. The stokes shift is enhanced on the Zn- and Se-rich side of $Zn_xHg_{1-x}Se_yS_{1-y}$ nanocrystals, implementing for the optical filters. Finally, these insights will be crucial in supporting the design of optoelectronic nanodevices and enabling the capability to accurately forecast the generation of polarized photon entanglement in the active pitch of quantum technology.

Acknowledgment

The author would like to acknowledge the support from Department of Physics, Faculty of Science, Ubon Ratchathani University, Thailand.

References

Bawendi, M. G. (2000). Optical gain and stimulated emission in nanocrystal quantum dots. **Science**, 290(5490), 314–317.

Benson, O., Santori, C., Pelton, M. and Yamamoto, Y. (2000). Regulated and entangled photons from a single quantum dot. **Physical Review Letters**, 84(11), 2513–2516.

Boykin, T. B. (2009). Recent developments in tight-binding approaches for nanowires. *Journal of* **Computational Electronics**, 8(2), 142–152.

Boykin, T. B., Luisier, M., Schenk, A., Kharche, N. and Klimeck, G. (2007). The electronic structure and transmission characteristics of disordered AlGaAs nanowires. **IEEE Transactions on Nanotechnology**, 6(1), 43–47.

Olguin, D., Baquero, R. and de Coss, R.. (2001). The band gap of II-VI ternary alloys in a tight-binding description. **Revista Mexicana de Fisica**, 47(1), 43-49

De Oliveira, E. L., Albuquerque, E. L., de Sousa, J. S., Farias, G. A., and Peeters, F. M. (2012). Configuration-interaction excitonic absorption in small Si/Ge and Ge/Si Core/Shell nanocrystals. **The Journal of Physical Chemistry C**, 116(7), 4399–4407.

Deng, Z. and Guyot-Sionnest, P. (2016). Intraband luminescence from HgSe/CdS core/shell quantum dots. **ACS Nano**, 10(2), 2121–2127.

Efros, A. L., Rosen, M., Kuno, M., Nirmal, M., Norris, D. J. and Bawendi, M. (1996). Band-edge exciton in quantum dots of semiconductors with a degenerate valence band: Dark and Bright Exciton States. **Physical Review B**, 54(7), 4843–4856.

Garcıa, A. E. Camacho A., Navarro H., Olguın D. and Baquero, R. (2000). Electronic band structure of II-VI quaternary alloys in a tight-binding approach. **Revista Mexicana de Física**, 46(3), 249-252

Hara, K., Machimura, H., Usui, M., Munekata, H., Kukimoto, H. and Yoshino, J. (1995). Gas-source molecular beam epitaxy of wide-band-gap $Zn_{1-x}Hg_xSe$ (x=0–0.14). **Applied Physics Letters**, 66(24), 3337–3339.

Hara, K., Yamamoto, K., Eguchi, Y., Usui, M., Munekata, H. and Kukimoto, H. (1996). Optical properties of wide bandgap ZnHgSSe layers grown by molecular beam epitaxy. **Journal of Crystal Growth**, 159(1-4), 45–49.

Hara, K., S. Haneda, Y. Eguchi and H. Munekata. (1998). Wide band-gap ZnHgSSe for visible lasers. **Journal of Crystal Growth**, 184-185, 610-613.

Butler, J.M. (2011). Advanced topics in forensic DNA typing: Methodology. California: Academic Press.

Klimov, V. I., Mikhailovsky, A. A., Xu, S., Malko, A., Hollingsworth, J. A., Leatherdale, C. A., Eisler, H.-J. and

Korgel, B. A. and Monbouquette, H. G. (2000). Controlled synthesis of mixed core and layered (Zn,Cd)S and (Hg,Cd)S nanocrystals within phosphatidylcholine vesicles. **Langmuir**, 16(8), 3588–3594.

Korkusinski, M. and Hawrylak, P. (2013). Atomistic theory of emission from dark excitons in self-assembled Quantum Dots. **Physical Review B**, 87(11), 115310-115320.

Lan, G.-Y., Lin, Y.-W., Lin, Z.-H. and Chang, H.-T. (2010). Synthesis and characterization of $Zn_xHG_{1-x}Se_yS_{1-y}$ quantum dots. **Journal of Nanoparticle Research**, 12(4), 1377–1388.

Lee, S., Oyafuso, F., von Allmen, P. and Klimeck, G. (2004). Boundary conditions for the electronic structure of finite-extent embedded semiconductor nanostructures. **Physical Review B**, 69(4), 045316-045323.

Malyk, O. P. (2009). Charge carrier scattering on the short-range potential of the crystal lattice defects in ZnCdTe, ZnHgSe and ZnHgTe. **Physica B: Condensed Matter**, 404(23-24), 5022–5024.

Mourad, D. and Czycholl, G. (2010). Multiband tight-binding theory of disordered $A_xB_{1-x}C$ Semiconductor Quantum Dots. **The European Physical Journal B**, 78(4), 497–507.

Nestoklon, M. O., Benchamekh, R. and Voisin, P. (2016). Virtual crystal description of III–V semiconductor alloys in the tight binding approach. **Journal of Physics: Condensed Matter**, 28(30), 305801.

Qi, L. and Gao, X. (2008). Quantum dot–amphipol nanocomplex for intracellular delivery and real-time imaging of siRNA. **ACS Nano**, 2(7), 1403–1410.

Reboredo, F. A., Franceschetti, A. and Zunger, A. (2000). Dark excitons due to direct coulomb interactions in silicon quantum dots. **Physical Review B**, 61(19), 13073–13087.

Schulz, S., Schumacher, S. and Czycholl, G. (2006). Tight-binding model for semiconductor quantum dots with a wurtzite crystal structure: From one-particle properties to coulomb correlations and optical spectra. **Physical Review B**, 73(24), 245327- 245341.

Shen, G. and Guyot-Sionnest, P. (2016). HgS and HgS/CdS colloidal quantum dots with infrared intraband transitions and emergence of a surface plasmon. **The Journal of Physical Chemistry C**, 120(21), 11744–11753.

Shen, G., Chen, M. and Guyot-Sionnest, P. (2017). Synthesis of nonaggregating HgTe colloidal quantum dots and the emergence of air-stable N-doping. **The Journal of Physical Chemistry Letters**, 8(10), 2224–2228.

Sheng, W., Cheng, S.-J. and Hawrylak, P. (2005). Multiband theory of multi-exciton complexes in self-assembled Quantum Dots. **Physical Review B**, 71(3), 035316- 035324.

Slater, J. C. and Koster, G. F. (1954). Simplified LCAO method for the periodic potential problem. **Physical Review**, 94(6), 1498–1524.

Smith, A. and Nie, S. (2009). Next-generation Quantum Dots. **Nature Biotechnology**, 27(8), 732–733.

Stathopoulos, A. and McCombs, J. R. (2010). PRIMME: preconditioned iterative multimethod eigensolver—methods and software description. **ACM Transactions on Mathematical Software**, 37(2), 1–30.

Sukkabot, W. (2016). Atomistic tight-binding computations in structural and optical properties of Cdse/ZnSe/ZnS core/multi-shell Nanocrystals. **Superlattices and Microstructures**, 95, 71–77.

Sukkabot, W. (2016). Atomistic tight-binding computations of excitonic fine structure splitting in CdSe/ZnSe type-I and ZnSe/CdSe invert type-I core/Shell Nanocrystals. **Materials Science in Semiconductor Processing**, 47, 57–61.

Sukkabot, W. (2016). Excitonic fine structure splitting in ZnTe/ZnX (x = S and SE) core/shell nanocrystals: Atomistic tight-binding theory. **Superlattices and Microstructures**, 91, 208–215.

Sun, Q., Wang, Y. A., Li, L. S., Wang, D., Zhu, T., Xu, J., Yang, C. and Li, Y. (2007). Bright, multicoloured light-emitting diodes based on quantum dots. **Nature Photonics**, 1(12), 717–722.

Vogl, P., Hjalmarson, H. P. and Dow, J. D. (1983). A semi-empirical tight-binding theory of the electronic structure of semiconductors†. **Journal of Physics and Chemistry of Solids**, 44(5), 365–378.

Wu, L., Romero, E. and Stathopoulos, A. (2017). PRIMME_SVDS: A high-performance preconditioned SVD solver for accurate large-scale computations. **SIAM Journal on Scientific Computing**, 39(5), S248–S271.

Zielinski, M. (2013). Valence band offset, strain and shape effects on confined states in self-assembled InAs/InP and InAs/GaAs Quantum Dots. **Journal of Physics: Condensed Matter**, 25(46), 465301-465316.

Zielinski, M., Korkusinski, M. and Hawrylak, P. (2010). Atomistic tight-binding theory of multiexciton complexes in a self-assembled InAs quantum dot. **Physical Review B**, 81(8), 085301-085312.

Zrazhevskiy, P. and Gao, X. (2009). Multifunctional Quantum Dots for personalized medicine. **Nano Today**, 4(5), 414–428.